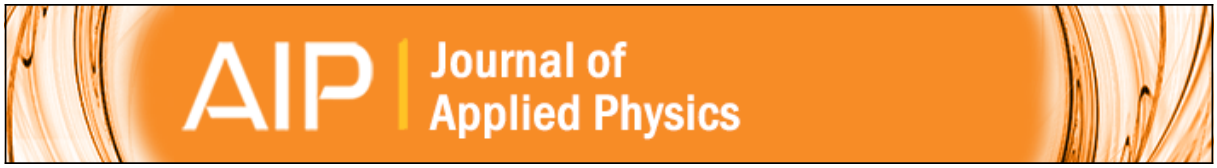

High-temperature healing of interfacial voids in GaAs wafer bonding

YewChung Sermon Wu, Po Chun Liu, R. S. Feigelson, and R. K. Route

Citation: Journal of Applied Physics **91**, 1973 (2002); doi: 10.1063/1.1430888
View online: http://dx.doi.org/10.1063/1.1430888
View Table of Contents: http://scitation.aip.org/content/aip/journal/jap/91/4?ver=pdfcov
Published by the AIP Publishing

Articles you may be interested in

Microstructure of GaAs/GaN interfaces produced by direct wafer fusion
Appl. Phys. Lett. **81**, 3152 (2002); 10.1063/1.1515116

Healing kinetics of interfacial voids in GaAs wafer bonding
Appl. Phys. Lett. **81**, 1429 (2002); 10.1063/1.1502194

Chemical investigations of GaAs wafer bonded interfaces
J. Appl. Phys. **90**, 5991 (2001); 10.1063/1.1416139

Interface structures in GaAs wafer bonding: Application to compliant substrates
Appl. Phys. Lett. **76**, 2674 (2000); 10.1063/1.126440

Defects, structure, and chemistry of InP–GaAs interfaces obtained by wafer bonding
J. Appl. Phys. **87**, 4135 (2000); 10.1063/1.373042

[This article is copyrighted as indicated in the article. Reuse of AIP content is subject to the terms at: http://scitation.aip.org/termsconditions. Downloaded to] IP: 140.113.38.11 On: Thu, 01 May 2014 06:26:57

High-temperature healing of interfacial voids in GaAs wafer bonding

YewChung Sermon Wu,[a] and Po Chun Liu
Department of Materials Science and Engineering, National Chiao Tung University, Hsinchu 300, Taiwan

R. S. Feigelson and R. K. Route
Center for Novel Optoelectronic Materials, Stanford University, California 94305

(Received 12 March 2001; accepted for publication 2 November 2001)

Artificial voids were introduced at bonding interfaces to study how processing parameters affected the healing mechanism of interfacial voids in GaAs wafer bonding. These voids were created by placing unpatterned wafers in contact with topographically patterned wafers. During the bonding process, crystallites formed within these voids and corresponded to bonded regions within the voids. Their formation depended strongly on the height of the surface irregularities at the wafer interfaces. When the void depth (h) was $\geqslant$200 nm, most of the crystallites were diamond shaped. The edges of the diamond features were elongated in the $\langle 100 \rangle$ direction. On the other hand, when the void depth was small ($h \leqslant 70$ nm), dendrites grew quickly in the $\langle 110 \rangle$ direction. © *2002 American Institute of Physics.* [DOI: 10.1063/1.1430888]

I. INTRODUCTION

Bonding of III–V semiconductors was originally developed for two-layer optoelectronic devices.[1–3] Based on these studies, a periodic structure of bonded GaAs wafers has been proposed for quasi-phase-matched (QPM) second harmonic generation (SHG).[4] Three kinds of defects that cause excess optical losses were identified in these structures: (1)bulk defects, (2)surface defects, and (3)interfacial defects.[5,6] The causes of bulk and surface defects in GaAs are complicated. It is well known from the extensive literature in the field that these defects include dislocations, impurities, vacancies, interstitials, precipitates, and antisite defects.[5,7] Interfacial defects, such as voids and inclusions, are caused by natural topographical irregularities, surface contamination, solvent residues, and trapped gases between the wafers. Most inclusions could be eliminated by the solvent-cleaning and heating cycles.[5] Interfacial voids, however, are inevitable because atomically smooth wafers are not available. Fortunately, these voids can be reduced by (1)increasing the compressive pressure at a given bonding temperature or (2)increasing the bonding time and temperature. After bonding, IR transmission microscopy revealed two kinds of bright features(crystallites) in these voids: diamond/rhombohedral geometry and dendrite geometry, as shown in Fig. 1. These crystallites represent bonded regions within the void space.[5]

Similar crystallites were found in studies of high-temperature crack healing in ceramic materials by Gupta,[8] and Wang *et al.*[9] The crack healing process and theory have been studied for many years because healing can result in a partial or complete recovery of the strength of these materials. Moreover, the morphological changes and transport mechanisms in crack healing were found to bear significant similarities to those in the GaAs wafer bonding processes. As a result, the research findings in crack healing were applied in the studies of the interfacial defects in wafer bonded GaAs.

Four stages have been identified in the ceramic crack-healing process:(a)a continuous regression of the void from the void tip or a discontinuous pinching-off of the void along the length of the void, (b)cylinderization of the voids, (c)breakup of the cylindrical voids into rows of isolated pores, and (d)shrinkage or growth of isolated pores. The last two stages have been well documented in the literature and the breakup of cylindrical pores has been analyzed by Nichols and Mullins.[10,11] However, the understanding of the first two stages is very limited. Gupta[8] proposed that the first stage would proceed through continuous regression or discontinuous pinching-off, depending on the stress state in the material. If the material remains stress-free after the introduction of a void, regression will predominate; if the material retains the residual compression stress, crack pinching will prevail.

Several methods have been used to study the first stage of ceramic crack healing. To control crack geometry, Rodel, Glaeser, and Powers[12–14] introduced cracks (voids) by bonding topographically patterned sapphire wafers to flat sapphire surfaces at elevated temperatures. They found that lots of crystallites formed in the void were initiated by the pinching-off mechanism, regardless of the applied stress. This result was not consistent with Gupta's assertion.

A similar approach has been used in this work to study the first healing stage of interfacial voids in GaAs wafer bonding, especially the formation of crystallites inside the voids.

II. EXPERIMENTAL PROCEDURE

Undoped semi-insulating (100)GaAs wafers polished on both sides were used in this study. To understand the effect of surface irregularities on the GaAs bonding mechanism, the atomic scale surface roughness of as-received wafers in a $5 \times 5 \mu m^2$ area was measured using atomic force microscopy

[a]Author to whom correspondence should be addressed; electronic mail: sermonwu@stanfordalumni.org

 © 2002 American Institute of Physics
[This article is copyrighted as indicated in the article. Reuse of AIP content is subject to the terms at: http://scitation.aip.org/termsconditions. Downloaded to] IP: 140.113.38.11 On: Thu, 01 May 2014 06:26:57

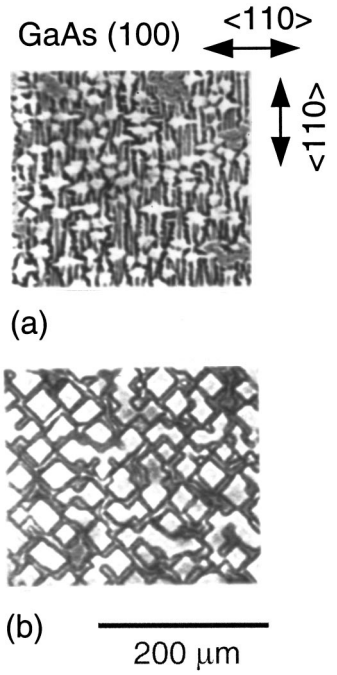

FIG. 1. Two kinds of features formed at the interface between bonded GaAs wafers: (a) dendrite and (b) diamond.

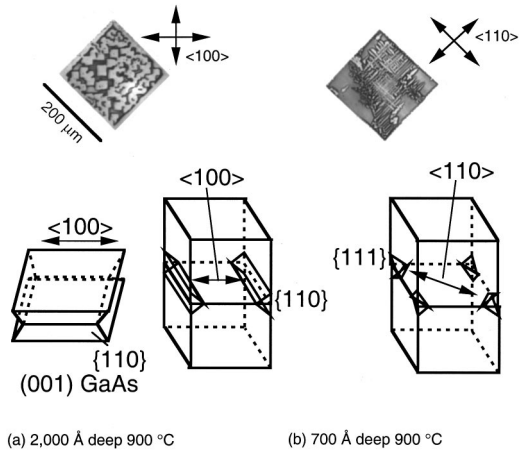

FIG. 2. Illustration of the (a) edges of the diamond and (b) cap of dendrite regions.

(AFM). Surfaces were very smooth with a typical peak-to-valley distance of only 1 nm. The surface waviness (long range flatness) in a $1\times1\text{cm}^2$ area was measured with a profilometer. The center of each wafer was generally much flatter than the periphery (edge), as expected. The peak-to-valley waviness at the center of a GaAs wafer was <100 nm, while that around the periphery was ≈ 300 nm.

An approach for making artificial voids similar to those in Refs. 12–14 was followed. It involved the creation of controlled voids in one wafer surface by etching it with photolithographically generated patterns with a solution of H_2SO_4, H_2O_2, and H_2O, and then bonding it to an unpatterned wafer. Using this approach, we were able to vary the void shape (disks, squares, and rectangles), size (ranging from 5 to 500 μm), and depth (ranging from 10 to 3000 nm), and therefore simulate the interfacial defects which are caused by natural topographical irregularities on the wafer surface. To create quasi-phase matched GaAs structures, each GaAs wafer was rotated by 180°.[4] This in turn creates a twin boundary at the interface.

The bonding conditions were described in detail in Ref. 5. Specimens bonded in the 850°–950 °C temperature range were periodically removed from the furnace to measure the morphology of the artificial voids and the crystallites within. They were then returned to the furnace to continue annealing.

III. RESULTS

A. Nucleation of crystallites in voids

After high temperature bonding, most crystallites formed in the void were initiated (nucleated) by the mechanism of pinching-off along the length of the void instead of by void regression, regardless of the void geometry. Even though various compressive stresses (0–3 MPa) were applied during bonding, most of the crystallites were nucleated by the pinching-off mechanism, as shown in Figs. 2–4. This result was not consistent with Gupta's assertion that void regression will predominate if the material remains stress-free after the introduction of a void.

B. Growth of crystallites in voids

The growth of crystallites had two principal morphologies: a dendrite geometry with dendritic arms in the ⟨110⟩

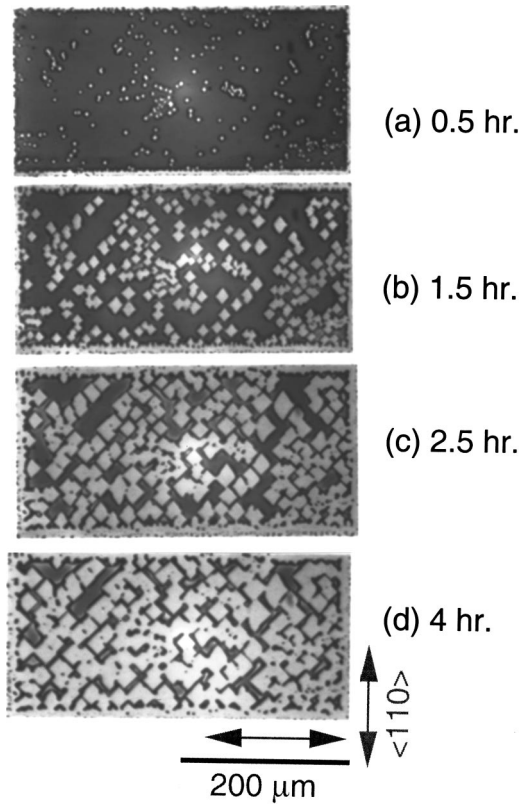

FIG. 3. IR transmission optical micrograph of 200 nm deep artificial voids in (100) GaAs wafers bonded at 950 °C for: (a) 0.5 h, (b) 1.5 h, (c) 2.5 h, and (d) 4 h.

[This article is copyrighted as indicated in the article. Reuse of AIP content is subject to the terms at: http://scitation.aip.org/termsconditions. Downloaded to] IP: 140.113.38.11 On: Thu, 01 May 2014 06:26:57

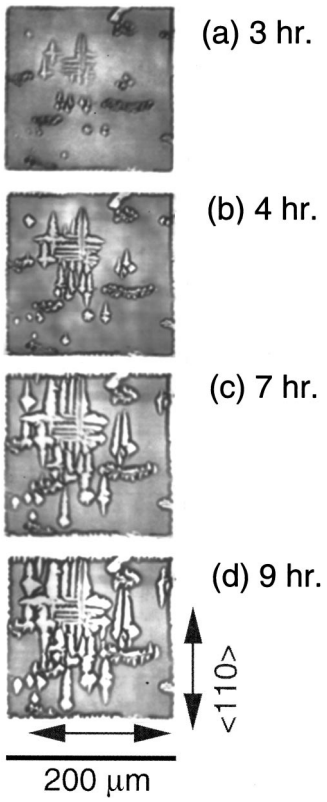

FIG. 4. IR transmission optical micrograph of 70 nm deep artificial voids in (001) GaAs wafers bonded at 900 °C for: (a) 3 h, (b) 4 h, (c) 7 h, and (d) 9 h.

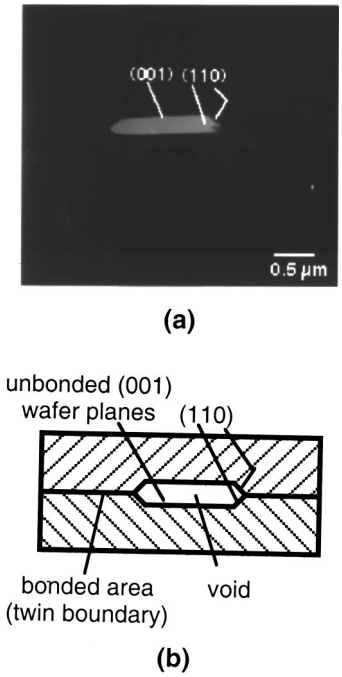

FIG. 5. (a) Cross-sectional TEM and (b) schematic illustration of the facet planes of a bonded (100) GaAs interface.

directions and a diamond/rhombohedral geometry with edges parallel to ⟨100⟩ directions, as shown in Fig. 2. The dendritic cap is bounded by {111} planes, while the diamond features were bounded by {110} planes which was verified by using transmission electron microscopy (TEM), as shown in Fig. 5.

The growth of these crystallites depended strongly on the depth of the void. When the void depth was 200 nm, diamond shapes were observed after the samples had been annealed at 950 °C for time periods $\geqslant$0.5 h, as shown in Fig. 3. The average growth rate before these features coalesced was in the 1–5 μm/h range. Their shapes were always diamond-like, regardless of the sizes of the crystallites. On the other hand, when the void depth was 70 nm, both diamond and dendrite features were observed after annealing at 900 °C for 3 h, as shown in Fig. 4. When the annealing time increased, the stability of the diamond edges broke down, and the dendritic arms grew from the corners of the diamond, i.e., in the ⟨110⟩ directions, as shown in Figs. 4 and 6. The average growth rate of the arm's length was around 7–8 μm/h, which is much higher than that of the arm's width (0.4–0.6 μm/h).

Neither crystallite growth rate was constant. However, the fraction of bonded regions (total area of the bright features in the void to the original void area) was found to increase with time. Thus, the void volume decreases with time.

IV. DISCUSSION

There are three steps related to mass-transport-induced crystallite growth in bonding areas: (1) decomposition from unbonded (001) wafer planes, (2) mass transport, and (3) deposition on the exposed facet planes, as shown in Fig. 7. The growth rate depends strongly on the driving force ΔG, which is given by

$$\Delta G = G_{\text{facet}} - G_{001},$$

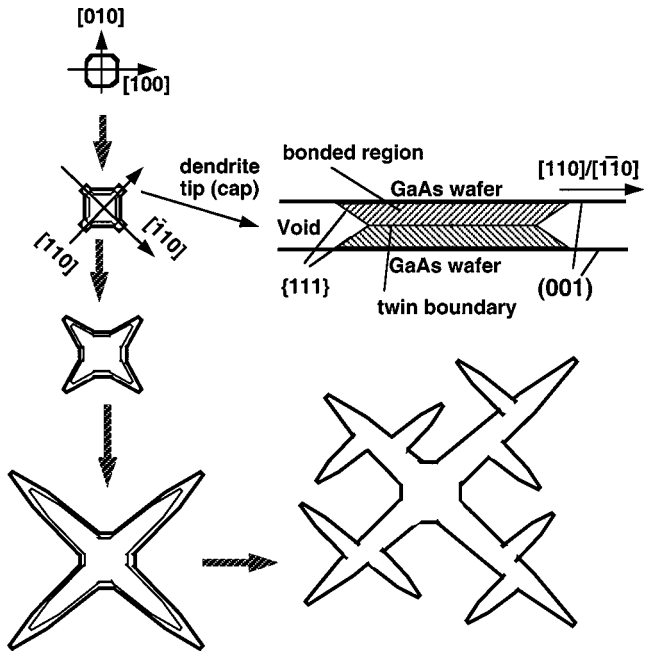

FIG. 6. Illustration of the instability of diamond edges in the 70 nm deep voids at high growth rates (driving forces) corresponding to small radii of curvature, and the growth of dendritic arms at the corners of the diamond, i.e., in the ⟨110⟩ direction.

[This article is copyrighted as indicated in the article. Reuse of AIP content is subject to the terms at: http://scitation.aip.org/termsconditions. Downloaded to] IP: 140.113.38.11 On: Thu, 01 May 2014 06:26:57

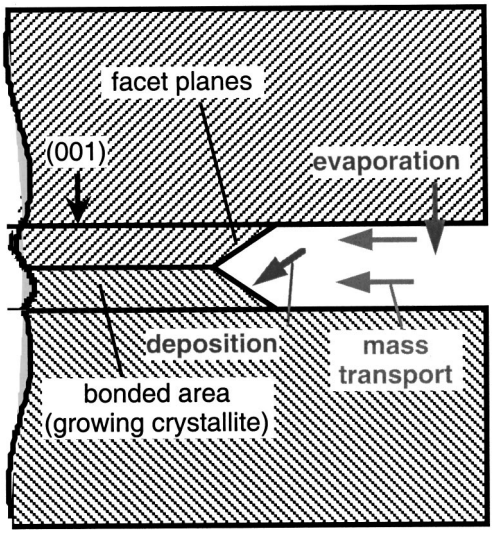

FIG. 7. Three steps related to the mass-transport-induced growth of the bonded areas: (1) decomposition, (2) mass transport, and (3) deposition on the bonded facet planes.

where G_{facet} is the free energy of the bonded facet planes (curved surfaces) and G_{001} is the free energy of the unbonded (001) wafer planes, as shown in Fig. 8.

As shown in Fig. 8, the two intersecting facets can be thought of as forming a curved surface in the Gibbs–Thomson treatment. The bulk driving force of a curved crystal is given by

$$\Delta G \approx k\frac{\gamma}{R} \approx 2k'\frac{\gamma}{h},$$

where γ is the free energy of the flat surface, R is the radius of curvature, h is the depth of the void, and k and k' are the geometry constants.

As shown in Fig. 8, ΔG is less than zero when R is negative. GaAs will decompose from the exposed unbonded (001) surfaces, transport to, and deposit on, the facet planes of crystallites. Since the driving force decreases with increasing radius of curvature, the crystallite growth rate decreases as the void depth increases. On the other hand, if the curvature is greater than zero, i.e., the free energy change is positive, GaAs will decompose from the bonded areas and deposit on the unbonded surfaces. The crystallite (bonded) areas are unstable and vanish. Therefore, the observed radius of curvature is always negative, as shown in Fig. 5.

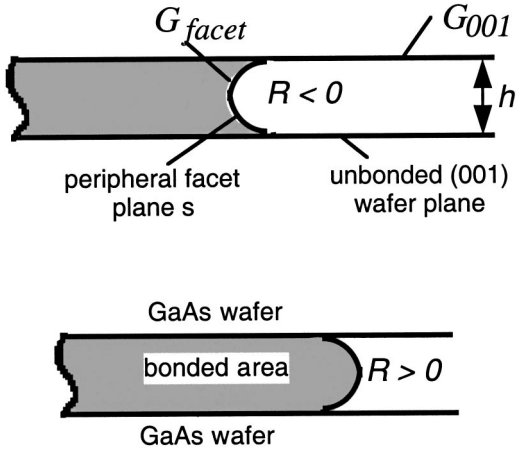

FIG. 8. Illustration of the relationship between free energy and driving force in mass-transport-induced growth of GaAs.

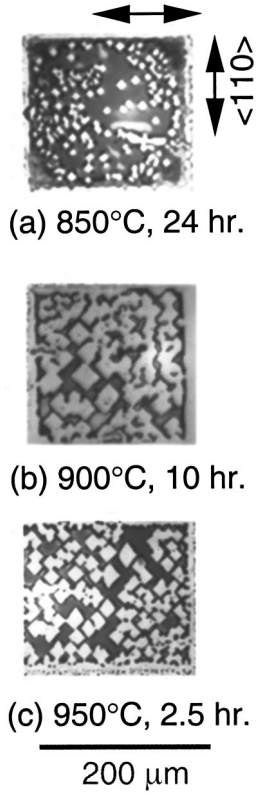

FIG. 9. IR transmission optical micrograph of artificial voids (originally 200 nm depth) in (001)GaAs wafers bonded at: (a) 850 °C for 24 h, (b) 900 °C for 10 h, (c) 950 °C for 2.5 h.

It is important to note that the observed shapes or ''growth habits'' of the crystallites are the results of surface energy anisotropy and/or growth rate anisotropy. The latter occurs when a particular crystal face affords easy atomic attachment and grows rapidly. Growth rate anisotropies can result in shapes that exaggerate actual surface energy anisotropies.[15] In practice these two effects can be difficult to separate, and are often simultaneously present.

By the Gibbs–Thomson calculation, when the void depth is large ($h \geqslant 200$ nm), the driving force is small. Regardless of the bonding temperature (850–950 °C) or bonding time, most crystallites were diamond-shaped (bounded by {110} planes), as shown in Figs. 2, 3 and 9. From this observation, the surface energies of the {110} faces seems to be lower than that of other planes. On the other hand, when the void depth was $\leqslant 70$ nm, the driving force became larger. In this case, the growth of GaAs crystallites results from growth rate anisotropy, and dendrites grow quickly along the fast growing ⟨110⟩ direction, regardless of the bonding temperature. This is shown in Figs. 4 and 10.

Both the reaction (decomposition and deposition) rate and mass transport rate increase with the bonding temperature. In consequence, the bonding fraction was significantly affected by the annealing temperature. As the temperature

[This article is copyrighted as indicated in the article. Reuse of AIP content is subject to the terms at: http://scitation.aip.org/termsconditions. Downloaded to] IP: 140.113.38.11 On: Thu, 01 May 2014 06:26:57

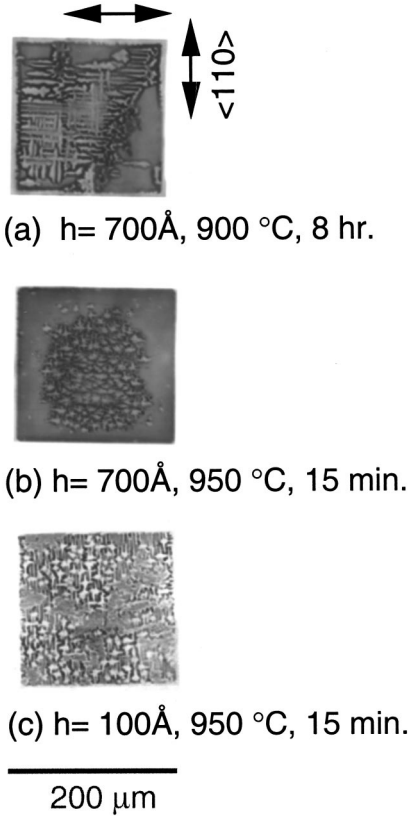

FIG. 10. Dendrite formation inside shallow artificial voids: (a) $h=70$ nm, 900 °C, 8 h, (b) $h=70$ nm, 950 °C, 15 min, (c) $h=10$ nm, 950 °C, 15 min.

increased, the time required to achieve the same bonding fraction diminished.

V. CONCLUSIONS

The effect of surface irregularities on the GaAs wafer bonding mechanism has been investigated. This was accomplished by placing unpatterned wafers in contact with topographically patterned wafers. After bonding, two kinds of crystallite were observed within these artificial voids: diamond-shaped and dendritic geometries. These two features resulted from both surface energy anisotropy and/or growth rate anisotropy. By the Gibbs–Thomson calculation, when the void depth h was $\geqslant$200 nm, the driving force for growth was small. The shape of crystallites results mainly from surface energy anisotropy. Regardless of the bonding temperature (850–950 °C) or time, most of the crystallites were diamond shaped. The edges of the diamond features were bounded by low surface energy {110} planes and elongated in the ⟨110⟩ direction. On the other hand, when the void depth was small ($h\leqslant$70nm), the driving force was larger. According to growth rate anisotropy, dendrites grew quickly in the ⟨110⟩ direction regardless of the bonding temperature, which was caused by fast growing {111} planes.

ACKNOWLEDGMENTS

This project was funded by National Science Council (NSC) of the Republic of China under Grant No. NSC89-2215-E009-075, and has benefited from facilities and equipment of Semiconductor Research Center of National Center for Materials Research at Chiao Tung University.

[1] F. A. Kish, D. A. Vanderwater, M. J. Peanasky, M. L. Ludowise, S. G. Hummel, and S. J. Rosner, Appl. Phys. Lett. **67**, 2060 (1995).
[2] Z. L. Liau, and D. E. Mull, Appl. Phys. Lett. **56**, 737 (1990).
[3] T. Akatsu, A. Plößs, H. Stenzel, and U. Gösele, J. Appl. Phys. **86**, 7146 (1999).
[4] L. A. Gordon, G. L. Woods, R. C. Eckardt, R. K. Route, R. S. Feigelson, M. M. Fejer, and R. Byer, Electron. Lett. **29**, 1942 (1993).
[5] Y. S. Wu, R. S. Feigelson, R. K. Route, D. Zheng, L. A. Gordon, M. M. Fejer, and R. Byer, J. Electrochem. Soc. **145**, 366 (1998).
[6] D. Zheng, L. A. Gordon, Y. S. Wu, R. K. Route, M. M. Fejer, R. L. Byer, and R. S. Feigelson, J. Electrochem. Soc. **144**, 1439 (1997).
[7] O. Oda, H. Yamamoto, M. Seiwa, G. Kano, T. Inoue, M. Mori, H. Shimakura, and M. Oyake, Semicond. Sci. Technol. **7**, A215 (1992).
[8] T. K. Gupta, *Structure and Properties of* MgO *and* Al_2O_3 *Ceramics* (American Ceramic Society, Columbus, OH, 1984), p. 750.
[9] Z. Wang, Y. Z. Li, M. P. Harmer, and Y. T. Chou, J. Am. Ceram. Soc. **75**, 1596 (1992).
[10] F. A. Nichols and W. W. Mullins, J. Appl. Phys. **36**, 1826 (1965).
[11] F. A. Nichols and W. W. Mullins, Trans. AIME **233**, 1840 (1965).
[12] J. Rodel and A. M. Glaeser, J. Am. Ceram. Soc. **73**, 592 (1990).
[13] J. D. Powers and A. M. Glaeser, J. Am. Ceram. Soc. **75**, 2547 (1992).
[14] J. D. Powers and A. M. Glaeser, J. Am. Ceram. Soc. **76**, 2225 (1993).
[15] Y. Chiang, D. Birnie III, and W. D. Kingery, *Physical Ceramics: Priciple for Ceramic Science and Engineering* (Wiley, New York, 1997), p. 354.

[This article is copyrighted as indicated in the article. Reuse of AIP content is subject to the terms at: http://scitation.aip.org/termsconditions. Downloaded to] IP: 140.113.38.11 On: Thu, 01 May 2014 06:26:57